Chemical Geology 402 (2015) 18–29

Contents lists available at ScienceDirect

Chemical Geology

journal homepage: www.elsevier.com/locate/chemgeo

Unusually low TEX_{86} values in the transitional zone between Pearl River estuary and coastal South China Sea: Impact of changing archaeal community composition

Jin-Xiang Wang [a,b,*], Yuli Wei [c,**], Peng Wang [a], Yiguo Hong [d], Chuanlun L. Zhang [a,***]

[a] State Key Laboratory of Marine Geology, Tongji University, Shanghai 200092, China
[b] Department of Marine Sciences, University of Georgia, Athens, GA 30602, USA
[c] Hadal Science and Technology Research Center, Shanghai Ocean University, Shanghai, China
[d] State Key Laboratory of Tropical Marine Environment, South China Sea Institute of Oceanography, Chinese Academy of Sciences, Guangzhou 510301, China

ARTICLE INFO

Article history:
Received 26 December 2014
Received in revised form 3 March 2015
Accepted 4 March 2015
Available online 11 March 2015

Editor: J. Fein

Keywords:
TEX_{86}
Isoprenoid GDGTs
The lower Pearl River
Estuary
South China Sea

ABSTRACT

TEX_{86}, calculated based on the distribution of isoprenoid glycerol dialkyl glycerol tetraethers (GDGTs), is used worldwide for paleotemperature reconstruction in marine and lacustrine environments. Recently, however, increasing evidence showed that TEX_{86} could be affected by multiple environmental variables. In this study, TEX_{86} was calculated for core and polar GDGTs obtained from water column and surface sediments in the lower Pearl River and its estuary. Together with previously published core GDGT data from the coastal and open South China Sea (SCS), a comparison was made between TEX_{86}-derived and satellite-based surface water temperature, which showed a TEX_{86}-temperature minimum that is considerably lower than winter satellite temperature in the transitional zone between the Pearl River estuary and the coastal SCS. TEX_{86} showed significantly positive correlation with GDGT-2 and GDGT-3 in this transitional zone, indicating that they are the primary compounds for the TEX_{86} bias toward cooler temperature. Lipid and molecular DNA data both indicate that the variation in archaeal community composition rather than water depth or seasonality is likely the crucial factor causing the deviation of TEX_{86} in the transitional area. Our study has implications for studies in ancient continental margins where unusually low TEX_{86} temperatures may be observed in the geological record.

1. Introduction

TEX_{86} is a (paleo-) sea surface temperature (SST) proxy based on the distribution of cyclic moieties of isoprenoidal glycerol dialkyl glycerol tetraethers (GDGTs, Fig. 1) of archaeal membrane lipids (Schouten et al., 2002). The calibration of TEX_{86} was made empirically using marine core top sediments collected globally (Schouten et al., 2002; Kim et al., 2008, 2010). To date, TEX_{86} has been applied to reconstruct paleo-SST in numerous cases (e.g. Liu et al., 2009; Zhang et al., 2014). However, with increasing application of TEX_{86} in different environments, it appeared that the TEX_{86} value could be affected by factors other than temperature (as reviewed in Pearson and Ingalls, 2013 and Schouten et al., 2013), such as 1) in situ production of GDGTs in sediments (Lipp and Hinrichs, 2009; Liu et al., 2011a; Dang et al., 2013, 2) input of GDGTs from the water column below the photic zone (Kim et al., 2012a; Huguet et al., 2007, 2) seasonal variability (Wuchter et al., 2006; Herfort et al., 2006a; Leider et al., 2010, 4) terrestrial input (Weijers et al., 2006; Herfort et al., 2006b, Zhu et al., 2011), and 5) preferential reservation of polar GDGTs (Schouten et al., 2012; Lengger et al., 2012). Further bias of TEX_{86} may be attributed to GDGTs produced from other groups of Archaea, such as marine group II (Lincoln et al., 2014) or methanotrophic (Weijers et al., 2011b; Zhang et al., 2011; Ho et al., 2014) *Euryarchaeota*, or group I.1b *Thaumarchaeota* of soil origin (Sinninghe Damsté et al., 2012).

Recently, analysis of surface sediments from coastal South China Sea (SCS) off the Pearl River (PR) estuary (water depth < 100 m) showed that TEX_{86}-derived temperatures were significantly lower than annual mean SST (Wei et al., 2011). This observation was confirmed by subsequent studies of Ge et al. (2013), Zhang et al. (2013), and Zhou et al. (2014), which examined the TEX_{86} temperature in the sediments from the same geographic region. The latter two studies favored an interpretation of winter signal imprinted by the low TEX_{86} values. This conclusion was supported by a previous study in the southern North Sea (Herfort et al., 2006a). In contrast, Castañeda et al. (2010) proposed that the TEX_{86} temperature in the coastal area of the Mediterranean Sea reflected summer signal during the Holocene. Leider et al. (2010) found

* Correspondence to: J.-X. Wang, Marine Sciences building, University of Georgia, Athens, GA 30605, USA. Tel.: +1 7065421605.
** Correspondence to: Y. Wei, Hadal Science and Technology Research Center, Shanghai Ocean University, 999 Huchenghuan Rd., Shanghai 201306, China. Tel.: +86 2161900730.
*** Correspondence to: C.L. Zhang, State Key Laboratory of Marine Geology, Tongji University, 1239 Siping Road, Shanghai 200092, China. Tel.: +86 2165982012.
E-mail addresses: jinxiang@uga.edu (J.-X. Wang), yl_wei@shou.edu.cn (Y. Wei), archaeazhang_1@tongji.edu.cn (C.L. Zhang).

http://dx.doi.org/10.1016/j.chemgeo.2015.03.002
0009-2541/

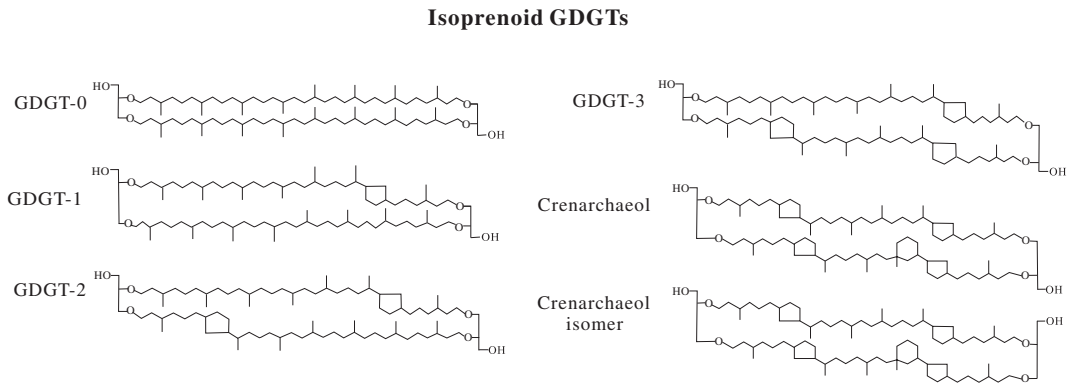

Fig. 1. Structures of archaeal core GDGTs described in the text.

that TEX_{86}-derived temperatures for the nearshore sites were similar to winter SST; whereas, at the most offshore sites, they were close to summer SST. In addition, several other investigations indicated that the TEX_{86}-derived temperatures from the surface sediments of coastal seas reflected temperature signals from different water depths (Lee et al., 2008; Lopes dos Santos et al., 2010). Therefore, it remains unclear what is the predominant factor that controls the variation of TEX_{86} in the coastal marine environment (water depth <200 m).

In this study we compared the distribution and abundance of archaeal membrane core lipids (CL or CL-GDGTs) and polar lipids (PL or PL-GDGTs) in the suspended particulate matters (SPM), surface sediments, and surrounding soils in the lower Pearl River and its estuary, and then examined the factors controlling the TEX_{86} signals in the estuary and coastal to open SCS by combining our data with those from Zhang et al. (2013), Ge et al. (2013), and Wei et al. (2011). Our results indicated that a TEX_{86} temperature minimum occurred in the

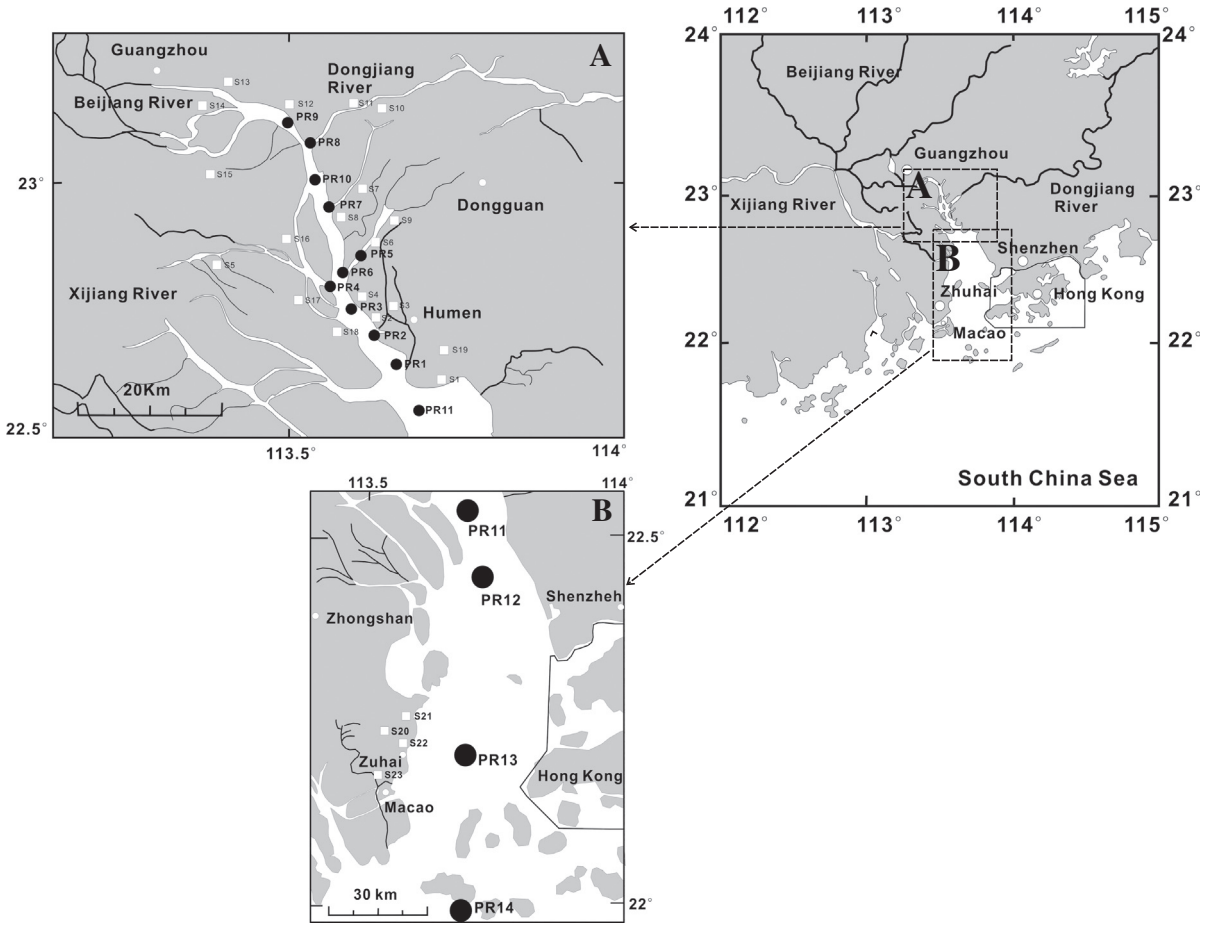

Fig. 2. Map of sampling locations of the lower Pearl River and the PR estuary. Panel A shows suspended particulate matter (SPM) samples from the water column of the lower Pearl River (black solid circles, PR1–PR10). Panel B shows SPM samples from the water column of the PR estuary (black solid circles, PR11–PR14). The surface sediment samples were collected at the same locations at which SPM samples were collected except for the station PR-13. Soil samples in the drainage basin of the lower PR and the PR estuary are shown in white squares. This map is modified from Zhang et al. (2012) and permission has been obtained from The Frontiers Publisher.

transitional zone between the PR estuary and coastal SCS. Together with molecular DNA data from SPM in the surface water, we suggested that the variation in archaeal community composition might be responsible for the unusually low TEX_{86}. Our study warns against the applicability of the TEX_{86} as a paleotemperature proxy for interpretation of low temperature events in ancient continental margins.

2. Material and methods

2.1. Sampling

The sampling procedures and analytic methods for water chemistry were described in detail in Zhang et al. (2012). Briefly, eighteen SPM samples and thirteen surface sediments were collected from the lower Pearl River (10 stations) and its estuary (4 stations) (Fig. 2) in the summer of 2010. SPM was collected from surface (ca. 1 m) of the lower Pearl River and from surface (ca. 1 m) and near the bottom (ca. 4–17 m) of the PR estuary. About 3–27 L of surface or bottom water were collected using a submersible pump and filtered onto ashed (450 °C, overnight) and pre-weighed glass-fiber filters (Whatman GF/F, 0.7 μm, 142 mm diameter) (Table 1). The pH, temperature, and salinity were determined in situ by a Horiba instrument (W-20XD, Kyoto, Japan) (Table 2).

Surface sediments (top ca. 10 cm) were collected using a grab sampler at all stations except for the estuarine station PR-13 at which a sediment sample was not collected (Fig. 2; Table 1). Twenty soil samples (from the top 5–10 cm) were also collected from within the catchment of the lower Pearl River and its estuary (Fig. 2).

All samples were frozen immediately in liquid nitrogen and kept at −80 °C in the laboratory before analysis. The same samples were used for simultaneous extraction of isoprenoid GDGTs and branched GDGTs; the results for branched GDGTs were reported previously (Zhang et al., 2012); in this study, we present the results of archaeal isoprenoid GDGTs.

Table 1
Basic information on geographic coordinates, water depths, volumes of water filtered (for SPM samples), and intervals of sediment samples from the lower Pearl River, the Pearl River estuary, and the coastal and open South China Sea (SCS).

Sample ID	Sampling date	Latitude (N)	Longitude (E)	Water depth (m)	SPM (L)	Sediment (cm)	Reference
Lower Pearl River							
PR-1[a]	Jul. 2010	22°47.126′	113°37.812′	8	3	Surface sedi. (0–10[c])	This study
PR-2	Jul. 2010	22°49.036′	113°36.926′	3	3	Surface sedi. (0–10)	This study
PR-3	Jul. 2010	22°50.339′	113°35.086′	15	6	Surface sedi. (0–10)	This study
PR-4	Jul. 2010	22°52.225′	113°32.462′	12	7	Surface sedi. (0–10)	This study
PR-5	Jul. 2010	22°54.392′	113°35.234′	12	7	Surface sedi. (0–10)	This study
PR–6	Jul. 2010	22°54.790′	113°33.809′	8	7	Surface sedi. (0–10)	This study
PR-7	Jul. 2010	22°58.252′	113°33.147′	7	7	Surface sedi. (0–10)	This study
PR-8	Jul. 2010	22°02.916′	113°31.388′	6	7	Surface sedi. (0–10)	This study
PR-9	Jul. 2010	22°03.478′	113°29.645′	15	8	Surface sedi. (0–10)	This study
PR-10	Jul. 2010	22°59.787′	113°31.842′	7	8	Surface sedi. (0–10)	This study
Pearl River estuary							
PR-11	Jul. 2010	22°42.967′	113°40.119′	5	SW[b]: 10 BW: 10	Surface sedi. (0–10)	This study
PR-12	Jul. 2010	22°35.698′	113°42.594′	10	SW: 11 BW: 11	Surface sedi. (0–10)	This study
PR-13	Jul. 2010	22°16.270′	113°41.921′	15	SW: 16 BW: 10	n.a.[d]	This study
PR-14	Jul. 2010	22°00.270′	113°41.986′	18	SW: 21 BW: 27	Surface sedi. (0–10)	This study
Coastal SCS							
A5	Aug. 2009	21.0°	115.0°	102	n.a.	Downcore (24)	Zhang et al. (2013)
A6	Aug. 2009	21.25°	114.7°	89	n.a.	Downcore (34)	Zhang et al. (2013)
A7	Aug. 2009	21.5°	114.5°	73	n.a.	Downcore (20)	Zhang et al. (2013)
A8	Aug. 2009	21.8°	114.2°	45	n.a.	Downcore (48)	Zhang et al. (2013)
A9	Aug. 2009	22.0°	114.0°	33	n.a.	Downcore (52)	Zhang et al. (2013)
A3	Aug. 2009	21°50.525′	114°23.163′	52	n.a.	Core top (0–5)	Ge et al. (2013)
E501	Aug. 2007	18°59.995′	110°41.835′	65	n.a.	Core top (0–5)	Ge et al. (2013)
E504	Aug. 2007	19°0.102′	111°18.096′	131	n.a.	Core top (0–5)	Ge et al. (2013)
E505	Aug. 2007	18°59.897′	111°29.029′	154	n.a.	Core top (0–5)	Ge et al. (2013)
Open SCS							
CF 11	Aug. 2007	19°43.341′	114°34.477′	1050	n.a.	Core top (0–5)	Ge et al. (2013)
CF 14	Aug. 2007	19°54.256′	115°12.971′	1120	n.a.	Core top (0–5)	Ge et al. (2013)
CF 15	Aug. 2007	19°59.581′	110°41.837′	1300	n.a.	Core top (0–5)	Ge et al. (2013)
CF 8	Aug. 2007	18°1.908′	111°3.710′	1548	n.a.	Core top (0–5)	Ge et al. (2013)
E407	Aug. 2007	18°29.810′	112°0.017′	1800	n.a.	Core top (0–5)	Ge et al. (2013)
CF 6	Aug. 2007	22°0.316′	119°30.060′	2441	n.a.	Core top (0–5)	Ge et al. (2013)
E422	Aug. 2007	18°0.341′	112°0.793′	2456	n.a.	Core top (0–5)	Ge et al. (2013)
MD05-2894	Apr./Mar. 2010	7°2.25′	111°33.11′	1982	n.a.	Core top (<5)	Wei et al. (2011)
MD05-2896	Apr./Mar. 2010	8°49.50′	111°26.47′	1657	n.a.	Core top (<5)	Wei et al. (2011)
MD05-2898	Apr./Mar. 2010	13°47.39′	112°11.03′	2395	n.a.	Core top (<5)	Wei et al. (2011)
MD05-2900	Apr./Mar. 2010	14°23.33′	110°41.47′	1455	n.a.	Core top (<5)	Wei et al. (2011)
MD05-2902	Apr./Mar. 2010	17°57.07′	114°57.33′	3697	n.a.	Core top (<5)	Wei et al. (2011)
MD05-2903	Apr./Mar. 2010	19°27.32′	116°15.15′	2066	n.a.	Core top (<5)	Wei et al. (2011)
MD05-2905	Apr./Mar. 2010	20°08.17′	117°21.61′	1647	n.a.	Core top (<5)	Wei et al. (2011)
HQ08-48PC	Apr./Mar. 2010	16°57.513′	110°31.581′	1474	n.a.	Core top (<5)	Wei et al. (2011)

[a] PR, the Pearl River, which is followed by station numbers. The sampling stations are shown in Fig. 2.
[b] "SW" or "BW" means "surface water" or "bottom water", respectively.
[c] Approximately 10 cm. See text for more details.
[d] Not available.

Table 2
Temperature (Temp.), pH, salinity (Sal.), and concentrations of total GDGTs and crenarchaeol for suspended particulate matters (SPM) in the water column and surface sediments collected from the lower Pearl River and its estuary[a]. The GDGTs from soil within the catchment of the lower Pearl River and its estuary are also included. All the lipid data are from this study.

Sample ID[b]		Temp. (°C)	pH	Sal. (%)	GDGTs_SPM (ng/l)[c] CL	CL-Cren.	PL	PL-Cren.	GDGTs_Sediments (ng/g) CL	CL-Cren.	PL	PL-Cren.	Sample ID	GDGTs_Soil (ng/g) CL	CL-Cren.	PL	PL-Cren.
Lower Pearl River													PR-Soil-1	8.7	5.6	2.6	0.6
PR-1		29.8	5.2	0.0	71.0	17.9	72.9	4.3	196.2	63.7	146.6	10.9	PR-Soil-2	45.7	27.3	3.5	0.1
PR-2		30.4	5.4	0.0	35.3	10.3	54.2	2.9	67.2	32.7	70.5	7.4	PR-Soil-3	322.5	111.0	141.9	21.0
PR-3		30.1	5.3	0.0	28.8	5.2	43.5	1.5	234.2	106.3	139.4	13.1	PR-Soil-4	43.3	25.4	3.2	0.1
PR-4		30.3	5.7	0.0	14.5	4.9	15.8	1.9	26.2	11.6	14.7	1.7	PR-Soil-5	30.2	12.5	6.4	0.7
PR-5		30.2	5.2	0.0	15.4	3.3	21.9	0.9	60.0	21.8	89.1	4.3	PR-Soil-6	16.8	7.1	3.5	0.6
PR-6		30.3	5.2	0.0	23.5	3.3	31.9	0.9	333.7	80.2	353.1	7.7	PR-Soil-7	5.0	2.0	0.7	0.1
PR-7		30.2	5.2	0.0	23.7	5.7	31.9	1.3	202.0	30.9	300.8	5.1	PR-Soil-8	12.0	5.0	2.3	0.6
PR-8		30.2	5.4	0.0	70.2	3.5	70.3	0.9	357.4	34.8	446.9	4.4	PR-Soil-9	335.7	178.9	19.1	1.7
PR-9		30.7	5.8	0.0	19.9	1.7	40.3	0.8	332.6	36.0	533.7	5.6	PR-Soil-10	83.3	21.6	16.8	1.9
PR-10		31.3	5.8	0.0	15.5	1.5	40.8	0.6	424.3	58.8	544.8	6.0	PR-Soil-11	7.1	4.1	1.7	0.4
Pearl River Estuary													PR-Soil-12	36.7	13.0	8.5	1.0
PR-11	S	30.1	6.3	0.1	7.6	3.0	9.2	2.7	66.4	40.2	20.9	5.4	PR-Soil-13	662.9	23.4	184.7	0.3
	B	30.0	6.3	0.1	7.4	2.7	8.8	2.2					PR-Soil-14	38.1	14.6	6.8	1.1
PR-12	S	31.0	6.7	0.0	22.4	13.6	36.0	8.7	228.6	122.9	82.7	17.2	PR-Soil-15	83.4	55.9	13.4	6.7
	B	28.0	7.3	2.2	37.9	17.3	64.1	36.2					PR-Soil-16	68.0	43.6	5.4	0.4
PR-13	S	30.5	7.4	0.8	7.4	4.6	26.5	16.5	n.a.[d]	n.a.	n.a.	n.a.	PR-Soil-17	5.1	2.7	3.4	1.0
	B	28.7	7.3	2.0	26.4	16.6	61.3	36.5					PR-Soil-18	71.7	35.6	11.2	4.9
PR-14	S	30.1	8.1	1.5	10.6	7.2	15.4	10.4	1119.0	675.9	189.8	77.6	PR-Soil-19	29.2	5.6	4.1	0.9
	B	24.2	7.6	3.6	41.1	26.4	31.3	17.1					PR-Soil-20	27.3	13.6	5.7	1.9

[a] Temperature, pH, and salinity are from Zhang et al. (2012).
[b] PR, the Pearl River, which is followed by station numbers; the letter "S" or "B" after station number means "surface" or "bottom", respectively. The sampling stations are shown in Fig. 2.
[c] CL, total core GDGTs; CL-Cren, Core Crenarchaeol; PL, total polar GDGTs; PL-Cren, Polar Crenarchaeol.
[d] Not available.

2.2. Analysis of archaeal isoprenoid GDGTs

Lipid extraction and separation of CL- and PL-GDGTs followed a modified Bligh and Dyer extraction procedure described in Zhang et al. (2012). Briefly, five grams of freeze-dried sediment or the cut pieces of a whole filter were extracted by sonication (10 min, 6×) with a mixture of methanol, dichloromethane (DCM) and phosphate buffer (pH 7.4) (2:1:0.8, v/v/v). The supernatants were combined and carefully evaporated to dryness under a steady stream of N_2 at 35 °C, re-dissolved in a small amount of n-hexane/ethylacetate (1:1,v/v) and separated into an apolar fraction that contained core lipids (CL-GDGTs) and a polar fraction that contained polar lipids (PL-GDGTs), using activated silica gel columns eluted sequentially with n-hexane/ethylacetate (1:1, v/v) and methanol. PL-GDGTs were treated in the following manner: half of the polar fractions (non-hydrolyzed polar fractions) were directly condensed, dissolved in n-hexane/isopropanol (99:1, v/v), and filtered using a PTFE filter that had a pore diameter of 0.45 μm; the other half (hydrolyzed polar fractions) was hydrolyzed (24 h, 70 °C) in 5% HCl/methanol (V/V). DCM and MilliQ water were added, and the DCM fraction was collected (repeated 4×). The DCM fraction was rinsed (6×) with MilliQ water in order to remove acid and dried under N_2 gas. The hydrolyzed fraction was also re-dissolved in n-hexane/isopropanol (99:1, v/v) and filtered through 0.45 μm PTFE filters.

The analysis of non-hydrolyzed polar fractions is to determine any carryover of CL-GDGTs into the polar fraction (Weijers et al., 2011a). In order to analyze PL-GDGTs as CL-GDGTs, the polar fraction was hydrolyzed to cleave off the polar head groups (Pitcher et al., 2009). Thus, the accurate yield of PL-GDGTs in the polar fraction needs to exclude any carryover of CL-GDGTs from the hydrolyzed polar fractions. Because the total polar GDGTs were calculated based on the difference of yield between hydrolyzed and non-hydrolyzed polar fractions, the precise composition of intact polar lipids was unknown. Thus, we used PL-GDGTs (polar lipid GDGTs) instead of IPL-GDGTs (intact polar lipid GDGTs) as described in Zhang et al. (2012).

All these fractions were analyzed using high performance liquid chromatography/atmospheric pressure chemical ionization-tandem mass spectrometry (HPLC/APCI-MS/MS), which was performed with an Agilent 1200 liquid chromatography equipped with an automatic injector coupled to QQQ 6460 MS and Mass Hunter LC-MS manager software using a procedure modified from Zhang et al. (2012) and Schouten et al. (2007). Separation was achieved with a Prevail Cyano column (2.1 mm × 150 mm, 3 μm; Alltech Deerifled, IL, USA) thermostated at 40 °C. Injection volume was 5 μl. GDGTs were first eluted isocratically with 90% A and 1% B for 5 min, followed by a linear gradient to 18% B in 45 min. Solvent was held for 10 min in 100% B and was then allowed to re-equilibrate in 90% A: 10% B over a period of 10 min. A represents n-hexane and B is a mixture solution of 90% n-hexane and 10% isopropanol.

Detection was performed using positive ion APCI. The $(M + H)^+$ diagnostic of each core isoprenoid GDGT (m/z 1302, 1300, 1298, 1296, 1294, 1292) was monitored via selected ion monitoring (SIM) mode. The conditions for Agilent 6460 ion source were as follows: nebulizer pressure 40 psi, vaporizer temperature 350 °C, drying gas (N_2) flow 5 L/min and temperature 250 °C, capillary voltage 3 kV, corona 4 μA. All fractions were quantified by adding a known amount of an internal C_{46} GDGT standard in the apolar and polar fractions (Huguet et al., 2006). The detection limit for GDGTs was 0.001 ng.

Indices based on the relative abundance of GDGTs were calculated as follows:

$$TEX_{86} = ([GDGT-2] + [GDGT-3] + [Cren.iso]) / ([GDGT-1] + [GDGT-2] + [GDGT-3] + [Cren.iso]) \quad (1)$$

$$TEX_{86}^{H} = \log(TEX_{86}) \quad (2)$$

$$SST = 68.4 \times TEX_{86}^{H} + 38.6 \quad (3)$$

(Schouten et al., 2002), (Kim et al., 2010) with the GDGT numbers corresponding to the GDGT structures in Fig. 1.

The calibrations of TEX_{86} by Kim et al. (2010) were chosen in this study because of its significant linear correlation with SST in the 15 °C–28 °C range (cf. Fig. 14 of Schouten et al., 2013) and lower standard error (<±2.5 °C). On the other hand, using the latest calibration of TEX_{86} based on the core top sediments of <200 m water depth (Kim et al., 2012a) would result in unrealistic values that are lower

than winter temperatures in surface water (Table S1 and Table S2). The analytical error for TEX_{86} was better than ±0.011 for all samples, which corresponded to about ±0.5 °C according to Kim et al. (2010).

2.3. DNA analysis

2.3.1. DNA isolation and amplification

Four SPM samples were selected to investigate the archaeal community composition along the lower Pearl River and its estuary, i.e. PR-4, PR-9, PR-12, and PR-14 (Fig. 2). Bulk DNA was extracted from SPM samples using PowerSoil™ DNA Isolation Kit (Mo Bio Laboratories, Carlsbad, CA). Archaeal 16S rRNA gene fragments were amplified using primers Arch21F (5′-TTCCGGTTG ATCCYGCCGCCGGA-3′) and Arch958R (5′-YCCGGC GTTGAMTCCAATT-3′) as previous described (DeLong, 1992). The conditions for amplification of archaeal 16S rRNA genes were as follows: initial denaturation at 95 °C for 3 min; 30 cycles of denaturing (1 min at 94 °C), annealing (1 min at 55 °C), and extension (1.5 min at 72 °C); and a final extension at 72 °C for 10 min. The PCR products were purified with a QIAquick PCR Purification kit (Qbiogene Inc., Irvine, CA).

2.3.2. Cloning analysis

The PCR product was ligated into the pMD-18 T vector (TaKaRa) and transformed into Escherichia coli DH5α competent cells. The transformed cells were plated on Luria-Bertani plates containing 100 μg/ml of ampicillin, 80 μg/ml of X-Gal (5-bromo-4-chloro-3-indolyl-β-D-galactopyranoside), and 0.5 mM IPTG (isopropyl-β-D-thiogalactopyranoside) and incubated overnight at 37 °C, Resulting PCR products were screened for correct size and purity by 1% agarose gel electrophoresis.

2.3.3. Phylogenetic analysis

The 16S rRNA gene sequences were grouped into operational taxonomic units (OTUs) with 3% distance cutoff with the DOTUR program (Schloss & Handelsman, 2005). Sequence similarity searches were performed using the BLAST network service of the NCBI database (http://www.ncbi.nlm.nih.gov/BLAST). The sequences were tested for chimeras by using the Ribosomal Database Project Chimera-Check program and were aligned with Clustal W (Thompson et al., 1997).

Accession number of nucleotide sequences. The sequences have been deposited in the GenBank database under accession numbers: KP769447–KP769519.

2.4. Satellite SST and air temperature

The satellite SST was obtained from the best SST (bSST) data sets from the NOAA advanced very-high-resolution radiometer (AVHRR) (version 5.0; http://pathfinder.nodc.noaa.gov) on a 4 km spatial resolution. Since the temperature reconstructed from the SPM was a snapshot signal, the mean SST of the sampling month (July) was extracted and averaged from the daily mean bSST for 30 days of July of 2010 using MATLAB. On the other hand, since the top ca. 10 cm sediments in the PR estuary were estimated to represent 6–10 yr deposition (Strong et al., 2012), the annual mean SST and winter mean SST used 8-year mean values of annual mean bSST (2003–2010) and monthly mean bSST (December–February), respectively. The mean air temperature of the month of July was 30 °C recorded near the city of Guangzhou (Liu et al., 2007).

2.5. Statistical analysis

Cluster analysis was performed on CL-GDGTs in the sediments from the lower Pearl River, the PR estuary, and the coastal and open SCS using the base program in R 2.12.1. Data for sediments from the coastal and open SCS were those of Wei et al. (2011), Ge et al. (2013), and Zhang et al. (2013). The relative abundance of CL-GDGTs from all samples was imported into R and the Euclidean method was used to compute the distance matrix and to generate a hierarchical clustering tree. The linear regression analysis was performed by iPython Notebook.

3. Results and discussion

3.1. CL- and PL-TEX_{86} temperatures in the lower Pearl River and soils

In the water column of the lower Pearl River, the CL-TEX_{86} temperatures (avg. 25.6 ± 0.6 °C, n = 10) were close to the satellite-based annual mean surface water temperature (SWT) (24.6 ± 0.1 °C) (Fig. 3a). However, the PL-TEX_{86} temperatures (avg. 27.6 ± 1.1 °C, n = 10) varied between the satellite-based annual and July mean SWT (Fig. 3b).

In the sediments of the lower Pearl River, the CL-TEX_{86} temperatures (avg. 25.2 ± 1.0 °C, n = 10) varied around the annual mean SWT as well (Fig. 3c); however, the PL-TEX_{86} temperatures (avg. 20.2 ± 2.9 °C, n = 10) were below the annual mean SWT and fluctuated around the winter mean SWT (20.4 ± 0.1 °C) (Fig. 3d; Fig. 4), which was in contrast to its fluctuation above the annual mean SWT in the SPM samples in the lower Pearl River (Fig. 3b).

In summary, the average values of the CL-TEX_{86} temperatures from either SPM or sediment samples were all close to annual mean SWT in the lower Pearl River (Fig. 4); whereas, the PL-TEX_{86} temperatures deviated from the annual mean SWT with the SPM samples exhibiting about 3 °C higher and the sediments 4 °C lower than the annual mean SWT (Fig. 4).

The TEX_{86} temperatures for soils from the catchment of the lower Pearl River and its estuary were also calculated (using Eq. (3)) in order to compare with the signals from the SPM and sediment samples. On average, the TEX_{86} values of the soil samples were significantly higher than those of surface water and surface sediments from the lower Pearl River (Suppl. Table S1, S2, and S3). When translating to temperatures, the CL-TEX_{86} temperatures (avg. 29.0 ± 2.4 °C, n = 20) and PL-TEX_{86} temperatures (avg. 29.6 ± 3.2 °C, n = 20) in the soils were correlated well with the July mean air temperature (30 °C), both of which were 1 °C–8 °C higher than those from the surface water SPM and the surface sediments in the lower Pearl River (Fig. 4).

The significant difference in TEX_{86} temperatures between soils and the SPM samples (Fig. 4) indicates a substantial amount of in situ production of GDGTs in the lower Pearl River, which is consistent with previous studies showing in situ production of crenarchaeol in the water column of the Amazon River (Kim et al., 2012b; Zell et al., 2013a, 2013b) and in the Yangtze River (Yang et al., 2013). Furthermore, the TEX_{86} temperature from PL-GDGTs in the SPM reflects water temperature during the collecting season (July). This is in line with previous observation that TEX_{86} temperature in the Yangtze River appeared to have a good correlation with in situ river temperature (Yang et al., 2013).

In contrast with the short time scale (ca. days or even months) of SPM in the water column, sediments represent a relatively long time accumulation, i.e. ca. 6–10 yrs for our sediment samples according to Strong et al. (2012). Hence, the CL- and PL-GDGTs in the surface sediments of the lower Pearl River may have multiple sources, including: 1) terrestrial input from surrounding soil, 2) vertical export from water column, 3) lateral transport from the upland, or 4) in situ production in the surface sediment.

Here we assess each of the above potential sources. 1) The substantial difference in TEX_{86} and the amount of total GDGTs between the surface sediments and soils (Fig. 4; Table 2) suggest that soil input in the surface sediment may be insignificant. 2) Due to the similarity in CL-TEX_{86} temperature between the SPM and surface sediments, most CL-GDGTs in the sediments are likely from the surface water. Yet, this interpretation cannot explain the offset of PL-TEX_{86} temperature between the SPM and the surface sediments. 3) Strong et al. (2012) suggested that most of terrestrial organic matter in the PR estuary were predominantly contributed by the cooler upland region based on the evidence that annual mean air temperature derived from the branched GDGTs-based proxies were cooler than a given annual mean air

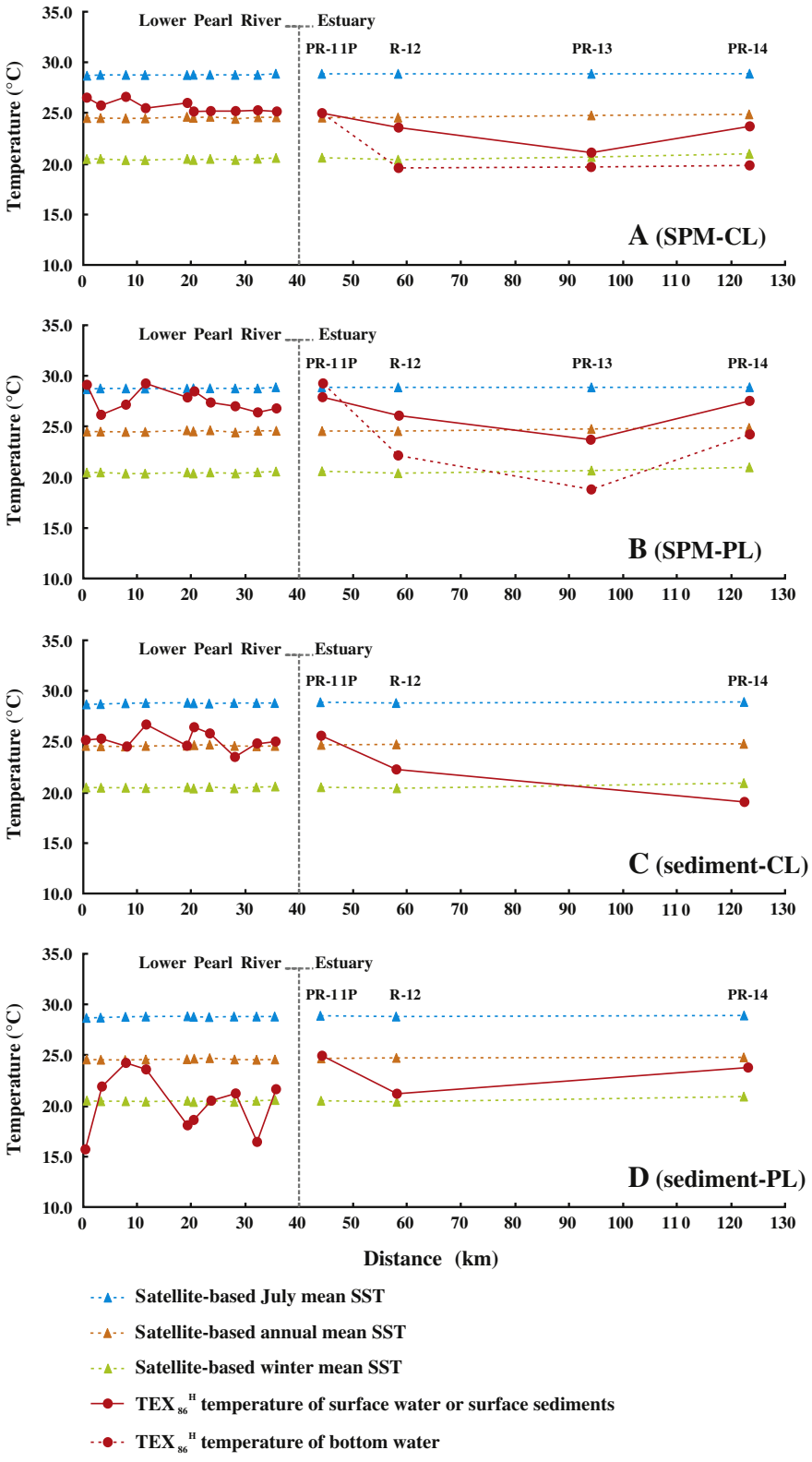

Fig. 3. Distance profiles of TEX_{86} temperature compared to the satellite-based annual mean SWT (yellow dashed line), satellite-based July mean SWT (blue dashed line), and satellite-based winter mean SWT (green dashed line). A: CL-TEX_{86} temperature from SPM in the surface water (red solid line) and bottom water (red dashed line); B: PL-TEX_{86} temperature from SPM in the surface water (red solid line) and bottom water (red dashed line); C: CL-TEX_{86} temperature in the surface sediments (red solid line); D: PL-TEX_{86} temperature in the surface sediments (red solid line). Triangular symbols are satellite-based temperatures at each sampling site; circular symbols are TEX_{86}-derived temperatures. PR-11, PR-12, PR-13, and PR-14 are station names in the Pearl River estuary. The distance profile starts from Guanghzou as 0 km; the lower Pearl River is 40 km long from Guangzhou to Humen (Fig. 2). (For interpretation of the references to color in this figure legend, the reader is referred to the web version of this article.)

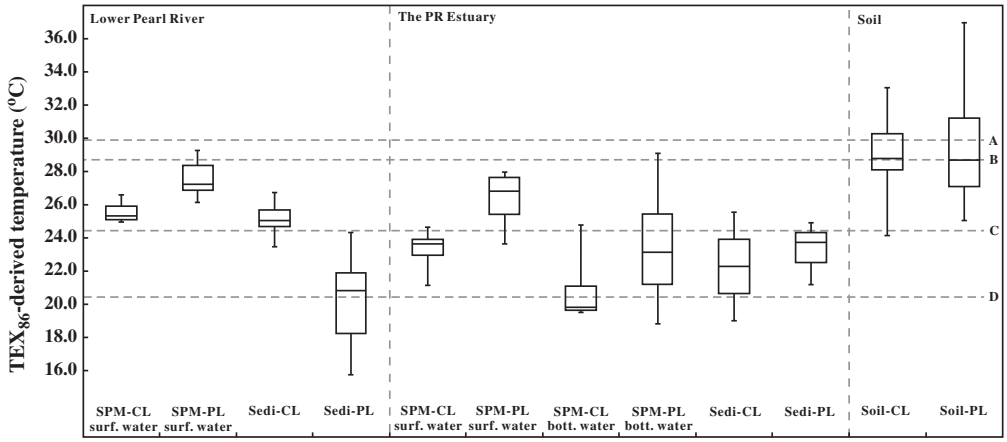

Fig. 4. TEX_{86}-derived temperatures from SPM samples, surface sediments and soils in comparison to satellite-based mean surface water temperatures (July, annual, and winter) and monthly mean air temperature in July in the sampling area. Dashed line A: Monthly mean air temperature in July (30 °C); dashed line B: Satellite-based July mean water surface temperature (28.78 ± 0.04 °C); dashed line C: Satellite-based annual mean water surface temperature (24.61 ± 0.09 °C); dashed line D: Satellite-based winter mean water surface temperature (20.49 ± 0.16 °C). CL, core lipids; PL, polar lipids.

temperature in the lowland Pearl River catchment. If that is the case, the PL-GDGTs in the surface sediment of the lower Pearl River may be derived from a cooler upland region because of the occurrence of low PL-TEX_{86} temperature (Figs. 3d & 4). This is counter intuitive as the CL-GDGTs should also register this cooler signal from upland, which is not the case in this study (more discussion in the next section). 4) Since the PL-TEX_{86} temperatures in the sediments were cooler than the annual mean SST even though sampling occurred in summer, it seems reasonable to assume that the dominant component of PL-GDGTs may be from in situ production in the sediments that are expected to have lower in situ temperature than the water column.

Overall, our data suggest that CL-TEX_{86} in the surface sediment is unlikely to be influenced by the relatively low abundance of PL-GDGTs produced in situ in the water column and surface sediments (Table 2). Consequently, the CL-TEX_{86} may have the potential to be employed as a palaeothermometer in the surface sediment of the lower Pearl River.

3.2. CL- and PL-TEX_{86} temperatures in the PR estuary

Variations in TEX_{86} temperature in the SPM and the surface sediments of the PR estuary were different from those in the lower Pearl River (Fig. 3). In the surface water of the PR estuary, the CL-TEX_{86} temperature fell between annual and winter mean SWT, whereas the PL-TEX_{86} temperature ranged between July and annual mean SWT (Fig. 3a & b). In the bottom water, the CL-TEX_{86} temperature approached the winter mean SWT, whereas PL-TEX_{86} temperature varied between annual and winter mean SWT (Fig. 3a & b). One exception was the PL-TEX_{86} temperature at the station PR-11, which was close to the satellite-based July mean SWT (Fig. 3b). Overall, the CL- and PL-TEX_{86} temperatures were consistently higher in the surface water than in the bottom water in the PR estuary, with the lowest average value occurring in the CL-GDGTs from the bottom water (Fig. 4).

In the sediments of the PR estuary, the CL-TEX_{86} temperature tended to decrease from close to the annual mean SWT at the station PR-11 to even slightly below the winter mean SWT at the station PR-14 (Fig. 3c). However, the PL-TEX_{86} temperature varied between the annual and winter mean SWT (Fig. 3d). Overall, CL- and PL-TEX_{86} temperatures were lower than the annual mean SWT, with the former being even lower than the winter temperature toward the open SCS (Fig. 4).

Comparison of CL- and PL-TEX_{86} in the SPM and the surface sediments of the PR estuary indicates that the CL-TEX_{86} signal in the surface sediments of the PR estuary is predominantly contributed by the CL-TEX_{86} in the water column. The seaward station, PR-14, appeared to be mainly contributed by CL-TEX_{86} signal in the bottom water (Fig. 3d), where, typically after the station PR-12, the water column seemed to be stratified according to the salinity and the water temperature (Table 2). This is consistent with previous interpretations that TEX_{86} signal in the surface sediment was mainly from suspended particulate organic matter in the water column in the southern North Sea (water depth <50 m) (Herfort et al., 2006a), and that, with increasing water depth, it even reflects the temperature of slightly deeper water in the Amazon shelf and slope (Zell et al., 2014). Further evidence comes from the comparison of the abundance of CL- and PL-crenarchaeol between the low Pearl River and its estuary. The abundance of crenarchaeol from the surface sediment of the PR estuary (CL = 279.7 ± 345.6 ng/g, n = 3; PL = 33.4 ± 38.7 ng/g, n = 3) was significantly higher than that from the lower Pearl River (CL = 47.7 ± 29.2 ng/g, n = 10; PL = 6.6 ± 3.3 ng/g, n = 10) (Table 2). This is consistent with the distribution of crenarchaeol in the SPM, i.e. the crenarchaeol concentration from the SPM in PR estuary (CL = 11.4 ± 6.4 ng/g, n = 8; PL = 16.3 ± 14.6 ng/g, n = 8) was up to 10-times higher than those from the lower Pear River (CL = 5.7 ± 5.0 ng/g, n = 10; PL = 1.6 ± 1.2 ng/g, n = 10) (Table 2), implying that the archaeal lipids in the surface sediments of the PR estuary are predominantly derived from the water column.

3.3. Possible mechanisms for the unusually low TEX_{86} in the transitional zone between the PR estuary and the coastal SCS

In the coastal area of northern South China Sea off the Pearl River estuary (water depth <200 m), the low temperature signals calculated based on the CL-TEX_{86} in the sediments were interpreted as impact of terrestrial input or reflecting winter temperature (Wei et al., 2011; Ge et al., 2013; Zhang et al., 2013; Zhou et al., 2014). In order to determine the predominant factor(s) causing a CL-TEX_{86} bias toward low temperature signal in the transitional zone between the PR estuary and coastal SCS, the CL-TEX_{86} values from this study, in combination with data sets from Wei et al. (2011), Ge et al. (2013), Zhang et al. (2013), were plotted against water depth (Fig. 5; Table 1). The results showed that TEX_{86} temperature did not reflect winter SWT as previous suggestions (Ge et al., 2013; Zhang et al., 2013; Zhou et al., 2014), but exhibited a trend of discrepancy between the TEX_{86} temperature estimates and the satellite-based winter temperatures in the transitional zone (at water depth of ca. 20–30 m) (Fig. 5). Although the TEX_{86} temperatures from Zhou et al. (2014) were relatively higher than those from other studies (Ge et al., 2013; Zhang et al., 2013) in the coastal SCS, which may result from different sampling season and/or different methods of lipid extraction, they decreased from above the winter SWT to below

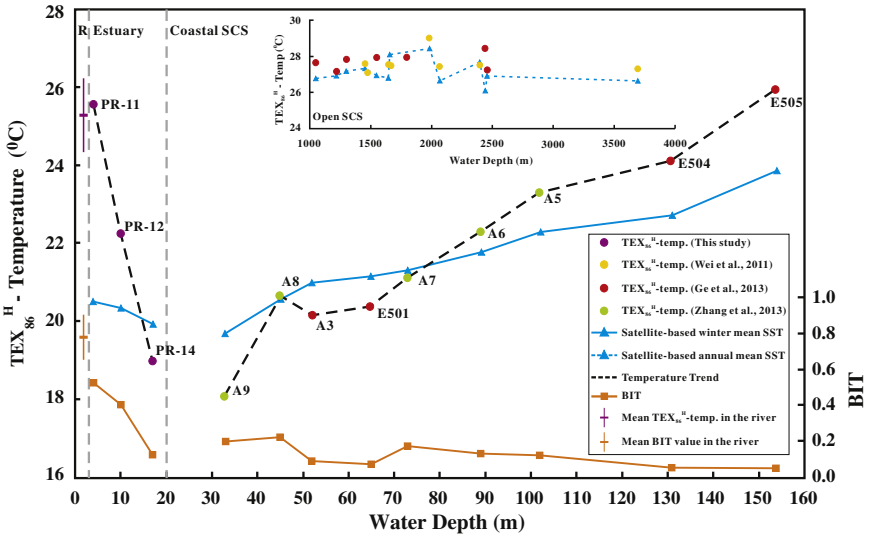

Fig. 5. The discrepancy between TEX_{86} temperature estimates (circles with station names) and satellite-based WST/SST (triangle) in the sediments from the transitional zone. The transitional zone is defined as an area from the PR estuary to the coastal SCS. The inset figure is TEX_{86} temperatures from core-tope sediments in the open South China Sea plotted against water depth. The horizontal purple bar represents the mean value of TEX_{86} temperatures in the surface sediments of the lower Pearl River (R); the vertical purple bar represents the range of TEX_{86} temperatures in the surface sediments of the lower Pearl River. BIT index (Branched and Isoprenoid Tetraether index) was proposed to evaluate terrestrial soil organic matter contribution to oceanic settings (Hopmans et al., 2004). The BIT data in the lower Pearl River (mean value, yellow bar) and the Pearl River estuary (yellow square) are from Zhang et al. (2012); those in the coastal sea (yellow square) are from Zhang et al. (2013) and Ge et al. (2013). The detailed sample information is in Table 1. (For interpretation of the references to color in this figure legend, the reader is referred to the web version of this article.)

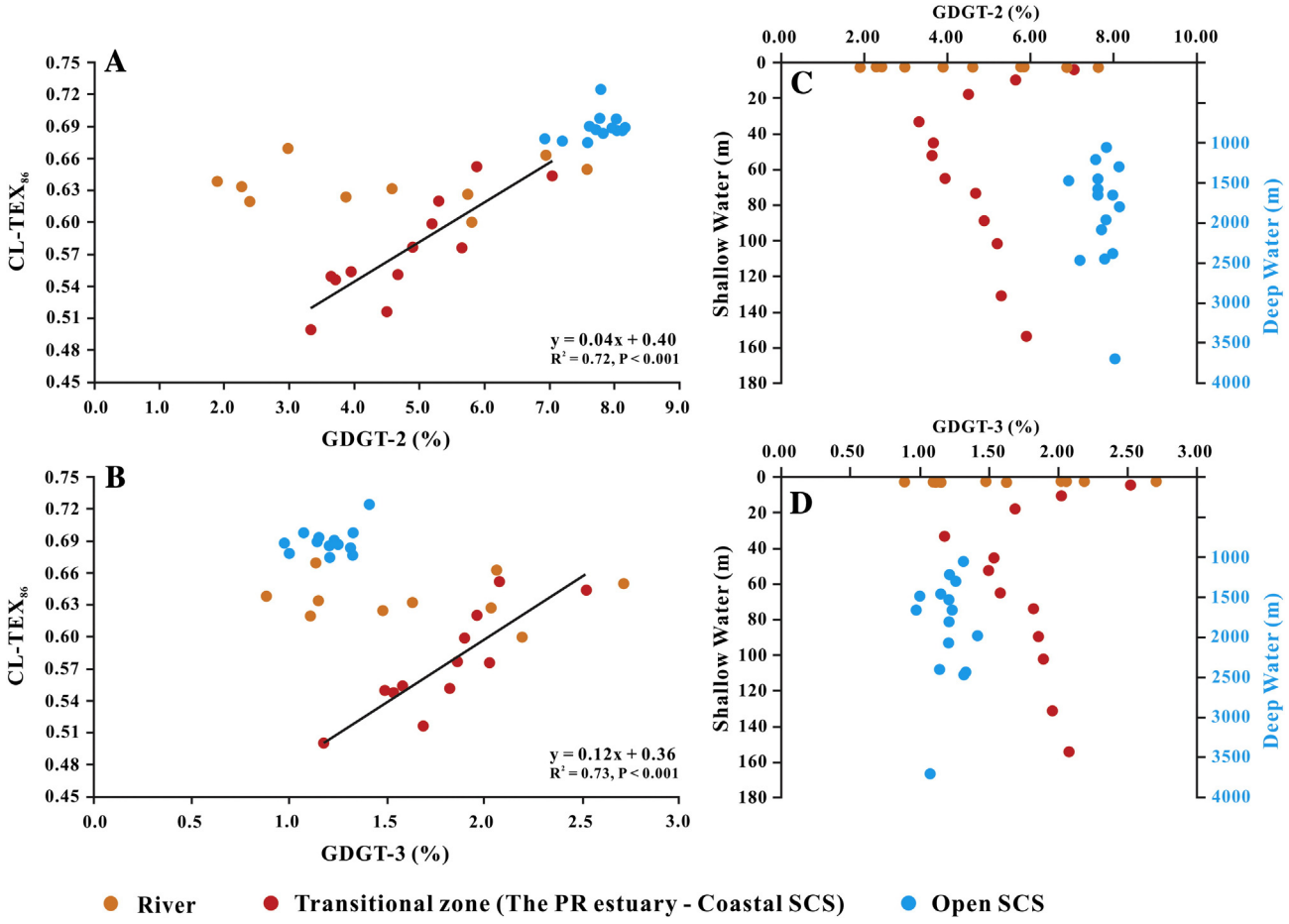

Fig. 6. Relationships between the fractional abundance of GDGT-2 and GDGT-3 and CL-TEX_{86} (A, B) and the distribution of fractional abundance of GDGT-2 and GDGT-3 versus water depth (C, D). Red solid circles represent sediments from the transitional zone (between estuary and the coastal SCS); yellow solid circles, river surface sediments; blue solid circles, core-tope sediments from the open SCS; solid line, linear regression of data from the transitional zone. The sediment data in the river and the estuary are from this study; the other sediment data (coastal and open SCS) are from Zhang et al. (2013), Ge et al. (2013), and Wei et al. (2011). The detailed sample information is in Table 1. (For interpretation of the references to color in this figure legend, the reader is referred to the web version of this article.)

Table 3
Linear regression analysis between the abundances of GDGT-2 or GDGT-3 and crenarhcaeol for core lipids (CL) and polar lipids (PL). PR, the lower Pearl River; PRE, the Pearl River estuary.

		CL		PL	
		PR (n = 10)	PRE (n = 8)	PR (n = 10)	PRE (n = 8)
GDGT-2	R	0.98	0.17	0.98	0.73
&	r^2	0.96	0.03	0.97	0.54
Crenarchaeol	P-value	0.000	0.689	0.000	0.038
GDGT-3	R	0.97	0.02	0.94	0.79
&	r^2	0.93	0.00	0.89	0.62
Crenarchaeol	P-value	0.000	0.962	0.000	0.020

the winter SWT as well (Table 1 of Zhou et al., 2014), showing a similar trend of discrepancy along the transitional zone (Fig. 5). However, in the open South China Sea (water depth of 1000–4000 m), the TEX_{86} temperature matched roughly the annual mean SST (Fig. 5). The inconsistency between TEX_{86} temperature and winter SWT in the sediments of coastal SCS suggests that seasonality seems unlikely to be a major factor controlling the GDGT distribution at water depth <200 m, particularly in the transitional zone between the PR estuary and the coastal SCS.

In order to evaluate which compounds may give rise to the deviation of TEX_{86} (Eq. (1)) toward the transitional zone between the PR estuary and the coastal SCS, fractional abundances (to total GDGTs) of the GDGT-1, GDGT-2, GDGT-3, and crenarchaeol regioisomer were assessed. The deviation of TEX_{86} in the transitional zone was linearly correlated with the fractional abundance of GDGT-2 and GDGT-3 (Fig. 6a & b) and reached the lowest points at the water depth of 20–30 m (Fig. 6c & d). Compared with the data from the open South China Sea (Wei et al., 2011; Ge et al., 2013), the fractional abundance of GDGT-2 was lower in the transitional zone (Fig. 6c), whereas the fractional abundance of GDGT-3 in the whole depth profile of the transitional zone was no less than that from the open South China Sea (Fig. 6d), suggesting that the GDGT-2 and GDGT-3 are key components causing the bias of TEX_{86} in the transitional zone. Similar observations were made by Taylor et al. (2013) and Hernandez-Sanchez et al. (2014) for other marine environments. On the other hand, the variation of GDGT-1 and crenarchaeol regioisomer exhibited no correlation with TEX_{86} in this region (data not shown), suggesting that these two compounds may have little impact on the variation of TEX_{86} in the transitional zone.

The unusually low CL-TEX_{86} in the transitional zone is an important observation in our study, which may be explained by four scenarios: 1) variation in CL-GDGT composition with water depth; 2) terrestrial input of CL-GDGTs; 3) preferential diagenesis of GDGTs; and 4) contribution of diverse members of the planktonic archaeal community. Regarding scenario 1, the TEX_{86} signal was not linearly correlated with water depth in the transitional zone (Fig. 5), which indicates that water depth is not a key factor controlling the variation of CL-TEX_{86}. For scenario 2, the comparison in TEX_{86} temperature between surface sediments in the lower Pearl River and its estuary and the soils (Fig. 4) has clearly indicated that terrestrial input had little impact on the distribution of TEX_{86} in the sediments of the PR estuary, which is also demonstrated by the low BIT values (<0.2) in the estuarine station PR-14 and the seaward coastal stations (Fig. 5). For scenario 3, although it is difficult to identify the degradation of GDGTs in the transitional zone, a recent study showed that the PR estuary was not characterized by extensive loss of organic matter through degradation (Strong et al., 2012). Furthermore, previous studies indicated that the distribution of core GDGTs in the sediments was not significantly affected by oxic degradation (Schouten et al., 2004; Kim et al., 2009; Turich et al., 2013).

Scenario 4 concerns with the variation in GDGTs within different thaumarchaeotal populations (e.g. fresh water vs. marine *Thaumarchaeota*) and the change in total archaeal community composition (e.g. *Euryarchaeota* vs. *Thaumarchaeota*) (Taylor et al., 2013; Hernandez-Sanchez et al., 2014 and refs. therein). The ratio of GDGT-2 to GDGT-3 ([2/3] ratio) was significantly lower in the PR estuary and coastal SCS than in the open South China Sea (Fig. 6). A similar observation using global modern core-top sediments and SPM in the modern water column was reported by Taylor et al. (2013). Hernandez-Sanchez et al. (2014) also noted the increase of the [2/3] ratio with water depth in subsurface and deep water of southeast Atlantic Ocean and suggested that this trend was related to the variation of thaumarchaeotal community composition, which arises from the evidence of the linear correlations between the concentrations of core GDGT-2 & 3 and core crenarchaeol, a known biomarker of *Thaumarchaeota* (Sinninghe Damsté et al., 2002).

In respect to the core lipids within the PR estuary, however, our data exhibited no correlation between the concentrations of GDGT-2 & GDGT-3 and crenarchaeol (Table 3). Even though both PL-GDGT-2

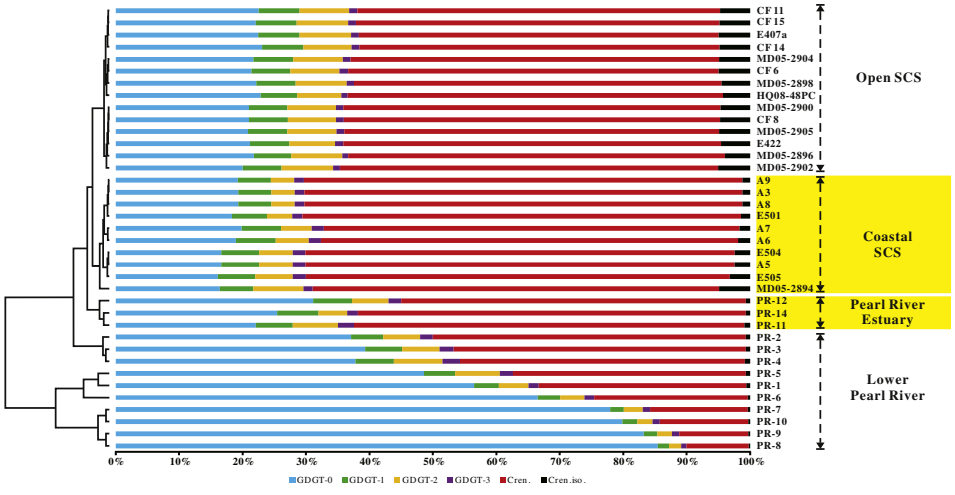

Fig. 7. Cluster analysis of the relative abundance of core GDGTs in the sediments from the lower Pearl River and its estuary, coastal SCS, and the open SCS. The data in the river and the estuary are from this study. The other data (coastal and open SCS) are from Wei et al. (2011) (HQ08-48PC, MD05-2894, MD05-2896, MD05-2398, MD05-2900, MD05-2902, MD05-2903, MD05-2905), Ge et al. (2013) (A3, CF6, CF8, CF11, CF14, CF15, E407a, E422, E501, E504, E505), Zhang et al. (2013) (A5, A6, A7, A8, A9). The detailed sample information shows in Table 1. The yellow highlight area represents the transitional zone. The structures of the GDGTs as in Fig. 1. (For interpretation of the references to color in this figure legend, the reader is referred to the web version of this article.)

and PL-GDGT-3 in the PR estuary appeared to be correlated with crenarchaeol to a certain degree, the correlation was not as strong as those exhibited in the lower Pearl River (Table 3), where PL-GDGTs were suggested as in situ production in the water column as discussed above. This indicates that *Thaumarchaeota* may not be the sole archaeal source to govern the distribution of GDGTs in the PR estuary given the insignificant impact of terrestrial input and preferential preservation.

Alternatively, the variation in archaeal community composition is likely the factor contributing to the unusually low TEX_{86} discrepancy in the surface sediments in the transitional zone. This is supported by the cluster analysis based on the distribution of CL-GDGTs in the sediments from different aquatic settings (Fig. 7). The cluster analysis identified four distinct aquatic settings, including 1) fresh water group (lower PR); 2) estuarine group (the PR estuary); 3) shallow water group (coastal South China Sea); and 4) deep water group (open South China Sea) (Fig. 7). The shallow water group (coastal SCS) was characterized by the highest fractional abundance of crenarchaeol and inconsistently distributed crenarchaeol regioisomer, whereas the estuarine group (the PR estuary) had a lower fractional abundance of crenarchaeol than the shallow water group, but a higher fractional abundance of GDGT-0 (Fig. 7). We hypothesize that changing characteristics of CL-GDGT distribution in the transitional zone between coastal SCS and the PR estuary is probably driven by the change in archaeal community composition.

To further evaluate this hypothesis, 16S rRNA gene clone libraries were analyzed to characterize the overall archaeal community in the surface water of the lower Pearl River and its estuary (Fig. 8 & Table S4). We assume that CL-GDGTs in the surface sediments are predominantly derived from the water column (Fig. 4). The results showed that the predominant archaeal population in the river water was *Methanosarcinales* in the upper end of the lower Pearl River (PR-9) and MCG in the lower end of the lower Pearl River (PR-4), which were distinct from the PR estuary (PR-12 & PR-14) where MG I.1a *Thaumarchaeota* predominantly occurred in the water column (Fig. 8). Intriguingly, MG II *Euryarchaeota* notably increased by 15% from the estuarine station PR-12 to PR-14; whereas it was absent in the riverine station PR-4 and PR-9 (Fig. 8). This is consistent with previous studies showing that MG II predominantly occurred in the surface water of the Pearl River estuary (Liu et al., 2014) and the Yangtze River estuary (Liu et al., 2011b). Xie et al. (2014) further demonstrated that salinity was the dominating factor controlling the change in archaeal community composition and their ecological function in the sediments of the lower Pearl River and its estuary based on the archaeal 16S rRNA gene from the surface sediments.

These results suggest that MG II *Euryarchaeota* may be another source in addition to *Thaumarchaeota* for the GDGT pool in the PR estuary. A similar observation was made by Turich et al. (2007) for other marine environments. Recently, Lincoln et al. (2014) presented evidence indicating that MG II *Euryarchaeota* were significant contributors to the GDGT pool (including crenarchaeol) in North Pacific Subtropical Gyre. Thus it is possible that MG II can be a major source of GDGTs in the marine system where *Euryarchaeota* occur abundantly, particularly in the coastal region (Pernthaler et al., 2002; Galand et al., 2010; Hugoni et al., 2013). On the other hand, the lack of MG II based on the genetic analysis in the surface sediments of coastal stations (Wang et al., 2014) may indicate that these organisms predominantly live in the water column and their DNA are decomposed after settling down in sediments, which thus cannot be used as evidence for excluding the contribution of MG II to the GDGT pool in the sediments at these locations. However, since none of the MG II *Euryarchaeota* has been isolated, their exact lipid profiles are unknown. Enrichment and isolation of MGII would be critical for resolving this issue in future research.

4. Conclusions

This study presents the spatial distribution of CL- and PL-TEX_{86} in the water column and sediment from the lower Pearl River to the PR estuary and coastal and open South China Sea. Terrestrial input of CL- and PL-GDGTs has little impact on the distribution and abundance of CL- and PL-GDGTs in the lower Pearl River and the PR estuary. In the water column, CL- and PL-GDGTs are largely from in situ production in the lower Pearl River and from a combination of fresh water and seawater in the PR estuary. However, the small fraction of PL-GDGTs in sediments does not seem to impact the distribution of CL-GDGTs. Thus, the CL-TEX_{86} in the surface sediments of lower Pearl River may have the potential to be used as a paleothermometer in the lower Pearl River. GDGT-2

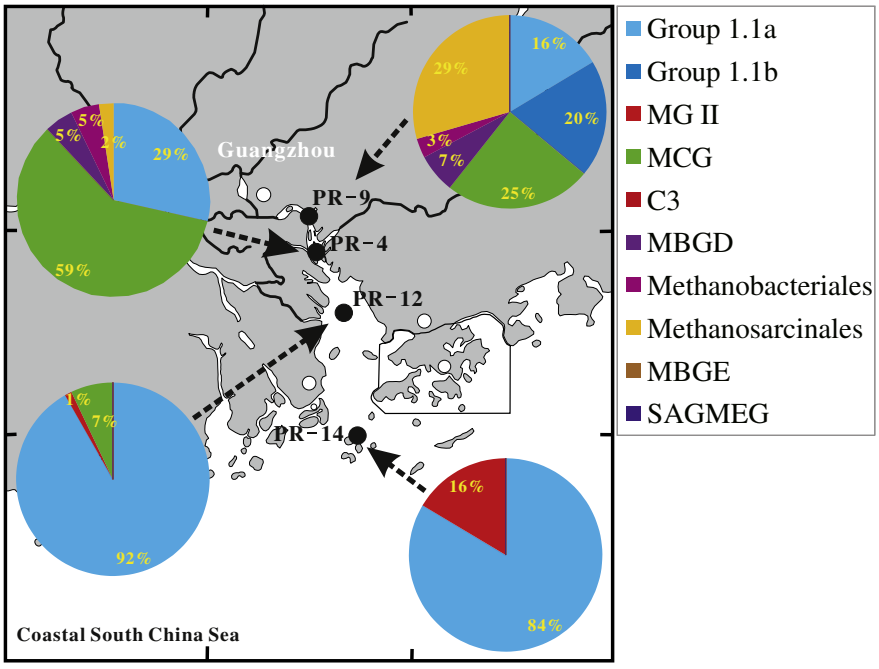

Fig. 8. The distribution of archaeal community composition based on 16S rRNA gene clone libraries from the lower Pearl River to the coastal SCS. PR-9 and PR-4 were from surface water of the lower Pearl River; PR-12 and PR-14 were from surface water of the PR estuary.

and GDGT-3 are crucial components toward unusually low TEX_{86} values in the transitional zone between the PR estuary and the coastal SCS (water depth ranging 10–200 m), which may be contributed by non-thaumarchaeotal species, such as Marine Group II *Euryarchaeota*. Consequently low temperature events based on TEX_{86} in ancient continental margins should be interpreted with extreme caution.

Acknowledgments

We thank Dai, L., Li, Y., Zhong, D., Wong C., and Shao L. for helping with the sampling and analysis of some of the samples collected for this study. Captain Deng was greatly appreciated for helping with the field experiments during the cruise. Chun Zhu and two anonymous reviewers provided excellent comments on an earlier version of the manuscript, which significantly improved the quality of the paper. Communication with James T. Hollibaugh and comments and advice from the handling editor (Jeremy Fein) of Chemical Geology are also greatly appreciated. This research was supported by the National Key Basic Research Program of China grant #2013CB955703 (CLZ), the South China Sea-Deep Program of the National Science Foundation of China Grant # 91028005 (CLZ), the State Key Program of National Natural Science of China Grant # 51439004 (YLW), special program for Hadal Science and Technology of Shanghai Ocean University Grant # HAST-S-2014-01 (YLW), the Doctoral Scientific Research Foundation of Shanghai Ocean University Grant # A2-0302-14-300066(YLW), the "National Thousand Talents" Program (CLZ) and the State Key Laboratory of Marine Geology of Tongji University.

Appendix A. Supplementary Data

Supplementary data to this article can be found online at http://dx.doi.org/10.1016/j.chemgeo.2015.03.002.

References

Castañeda, I.S., Schefuß, E., Pätzold, J., Sinninghe Damsté, J.S., Weldeab, S., Schouten, S., 2010. Millennial-scale sea surface temperature changes in the Eastern Mediterranean (Nile River Delta Region) over the last 27,000 years. Paleoceanography 25, PA1208. http://dx.doi.org/10.1029/2009PA001740.

Dang, H., Zhou, H., Yang, J., Ge, H., Jiao, N., Luan, X., Zhang, C.L., Klotz, M.G., 2013. Thaumarchaeotal signature gene distribution in sediments of the northern South China Sea: an indicator o the metabolic intersection of the marine carbon, nitrogen, and phosphorus cycles? Appl. Environ. Microbiol. 79, 2137–2147.

DeLong, E.F., 1992. Archaea in coastal marine environments. Proc. Natl. Acad. Sci. U. S. A. 89, 5685–5689.

Galand, P.E., Gutierrez-Provecho, C., Massana, R., Gasol, J., Casamayor, E.O., 2010. Interannual recurrence of archaeal assemblages in the coastal NW Mediterranean Sea. Limnol. Oceanogr. 55, 2117–2125.

Ge, H.M., Zhang, C.L., Dang, H.Y., Zhu, C., Jia, G.D., 2013. Distribution of tetraether lipids in surface sediments of the northern South China Sea: implications for TEX_{86} proxies. Geosci. Front. 4, 223–229.

Herfort, L., Schouten, S., Boon, J.P., Sinninghe Damsté, J.S., 2006a. Application of the TEX_{86} temperature proxy in the southern North Sea. Org. Geochem. 37, 1715–1726.

Herfort, L., Schouten, S., Boon, J.P., Woltering, M., Baas, M., Weijers, J.W.H., Sinninghe Damsté, J.S., 2006b. Characterization of transport and deposition of terrestrial organic matter in the southern North Sea using the BIT index. Limnol. Oceanogr. 51, 2196–2205.

Hernandez-Sanchez, M.T., Woodward, E.M.S., Taylor, K.W.R., Henderson, G.M., Pancost, R.D., 2014. Variations in GDGT distributions through the water column in the South East Atlantic Ocean. Geochim. Cosmochim. Acta 132, 337–348.

Ho, S.L., Mollenhauer, G., Fietz, S., Martinez-Garcia, A., Lamy, F., Rueda, G., Schipper, K., Meheust, M., Rosell-Mele, A., Stein, R., Tiedemann, R., 2014. Appraisal of TEX_{86} and TEX_{86}^{L} thermometries in subpolar and polar regions. Geochim. Cosmochim. Acta 131, 213–226.

Hopmans, E.C., Weijers, J.W.H., Schefuss, E., Herfort, L., Sinninghe Damsté, J.S., Schouten, S., 2004. A novel proxy for terrestrial organic matter in sediments based on branched and isoprenoid tetraether lipids. Earth Planet. Sci. Lett. 224, 107–116.

Hugoni, M., Taib, N., Debroas, D., Domaizon, I., Dufournel, I.J., Bronner, G., Salter, I., Agogue, H., Mary, I., Galand, P.E., 2013. Structure of the rare archaeal biosphere and seasonal dynamics of active ecotypes in surface coastal waters. Proc. Natl. Acad. Sci. U. S. A. 110 (15), 6004–6009.

Huguet, C., Hopmans, E.C., Febo-Ayala, W., Thompson, D.H., Sinninghe Damsté, J.S., Schouten, S., 2006. An improved method to determine the absolute abundance of glycerol dibiphytanyl glycerol tetraether lipids. Org. Geochem. 37, 1036–1041.

Huguet, C., Schimmelmann, A., Thunell, R., Lourens, L.J., Sinninghe Damsté, J.S., Schouten, S., 2007. A study of the TEX_{86} paleothermometer in the water column and sediments of the Santa Barbara Basin, California. Paleoceanography. http://dx.doi.org/10.1029/2006PA001310.

Kim, J.-H., Schouten, S., Hopmans, E.C., Donner, B., Sinninghe Damsté, J.S., 2008. Global core-top calibration of the TEX_{86} paleothermometer in the ocean. Geochim. Cosmochim. Acta 72, 1154–1173.

Kim, J.-H., Huguet, C., Zonneveld, K.A.F., Versteegh, G.J.M., Roeder, W., Sinninghe Damsté, J.S., Schouten, S., 2009. An experimental field study to test the stability of lipids used for the TEX_{86} and $U^{K'}_{37}$ palaeothermometers. Geochim. Cosmochim. Acta 73, 2888–2898.

Kim, J.-H., van der Meer, J., Schouten, S., Helmke, P., Willmott, V., Sangiorgi, F., Koç, N., Hopmans, E.C., Sinninghe Damsté, J.S., 2010. New indices and calibrations derived from the distribution of crenarchaeal isoprenoid tetraether lipids: implications for past sea surface temperature reconstructions. Geochim. Cosmochim. Acta 74, 4639–4654.

Kim, J.H., Romero, O.E., Lohmann, L., Donner, B., Laepple, T., Haam, E., Sinninghe Damsté, J.S., 2012a. Pronounced subsurface cooling of North Atlantic waters off Northwest Africa during Dansgaard–Oeschger interstadials. Earth Planet. Sci. Lett. 339–340, 95–102.

Kim, J.H., Zell, C., Moreira-Turcq, P., Pérez, M.A.P., Abril, G., Mortillaro, J.M., Weijers, J.W.H., Meziane, T., Sinninghe Damsté, J.S., 2012b. Tracing soil organic carbon in the lower Amazon River and its tributaries using GDGT distributions and bulk organic matter properties. Geochim. Cosmochim. Acta 90, 163–180.

Lee, K.Y., Kim, J.H., Wilke, I., Helmke, P., Schouten, S., 2008. A study of the alkenone, TEX_{86}, and planktonic foraminifera in the Benguela Upwelling System: implications for past sea surface temperature estimates. Geochem. Geophys. Geosyst. 9, Q10019. http://dx.doi.org/10.1029/2008GC002056.

Leider, A., Hinrichs, K.-U., Mollenhauer, G., Versteegh, G.J.M., 2010. Core-top calibration of the lipid-based $U^{K'}_{37}$ and TEX_{86} temperature proxies on the southern Italian shelf (SW Adriatic Sea, Gulf of Taranto). Earth Planet. Sci. Lett. 300, 112–114.

Lengger, S.K., Hopmans, E.C., Reichart, G.-J., Nierop, K.G.J., Sinninghe Damsté, J.S., Schouten, S., 2012. Distribution of core and intact polar glycerol dibiphytanyl glycerol tetraether lipids in the Arabian Sea Oxygen Minimum Zone. II: evidence for selective preservation and degradation in sediments and consequences for the TEX_{86}. Geochim. Cosmochim. Acta 98, 244–258.

Lincoln, S.A., Wai, B., Eppley, J.M., Church, M.J., Summons, R.E., DeLong, E.F., 2014. Planktonic Euryarchaeota are a significant source of archaeal tetraether lipids in the ocean. Proc. Natl. Acad. Sci. U. S. A. 111 (27), 9858–9863.

Lipp, J.S., Hinrichs, K.-U., 2009. Structural diversity and fate of intact polar lipids in marine sediments. Geochim. Cosmochim. Acta 73, 6816–6833.

Liu, Z., Colin, C., Phon Le, K., Tong, S., Chen, Z., Trentesaux, A., 2007. Climatic and tectonic controls on weathering in south China and Indochina Peninsula: clay mineralogical and geochemical investigations from the Pearl, Red, and Mekong drainage basins. Geochem. Geophys. Geosyst. 8, 1–18.

Liu, Z., Pagani, M., Zinniker, D., DeConto, R., Huber, M., Brinkhuis, H., Shah, S.R., Leckie, M., Pearson, A., 2009. Global cooling during the Eocene–Oligocene climate transition. Science 323, 1187–1190.

Liu, M., Xiao, T., Wu, Y., Zhou, F., Zhang, W., 2011a. Temporal distribution of the archaeal community in the Changjiang Estuary hypoxia area and the adjacente East China Sea as determined by denaturing gradiente gel electrophoresis and multivariate analysis. Can. J. Microbiol. 57, 504–513.

Liu, X.L., Lipp, J.S., Hinrichs, K.-U., 2011b. Distribution of intact and core GDGTs in marine sediments. Org. Geochem. 42, 368–375.

Liu, J., Yu, S., Zhao, M., He, B., Zhang, X.-H., 2014. Shifts in archaeaplankton community structure along ecological gradients of Pearl Estuary. FEMS Microbiol. Ecol. 90 (2), 424–435.

Lopes dos Santos, R., Prange, M., Castañeda, I.S., Schefuß, E., Mulitza, S., Schulz, M., Niedermeyer, E.M., Sinninghe Damsté, J.S., Schouten, S., 2010. Glacial–interglacial variability in Atlantic meridional overturning circulation and thermocline adjustments in the tropical North Atlantic. Earth Planet. Sci. Lett. 300, 407–414.

Pearson, A., Ingalls, A.E., 2013. Assessing the use of archaeal lipids as marine environmental proxies. Ann. Rev. Earth Planet. Sci. 41, 359–384.

Pernthaler, A., Preston, C.M., Pernthaler, J., DeLong, E.F., Amann, R., 2002. Comparison of fluorescently labeled oligonucleotide and polynucleotide probes for the detection of pelagic marine bacteria and archaea. Appl. Environ. Microbiol. 68, 661–667.

Pitcher, A., Hopmans, E.C., Schouten, S., Sinninghe Damsté, J.S., 2009. Separation of core and intact polar archaeal tetraether lipids using silica columns: insights into living and fossil biomass contributions. Org. Geochem. 40, 12–19.

Schloss, P.D., Handelsman, J., 2005. Introducing DOTUR, a computer program for defining operational taxonomic units and estimating species richness. Appl. Environ. Microbiol. 71, 1501–1506.

Schouten, S., Hopmans, E.C., Schefuß, E., Sinninghe Damsté, J.S., 2002. Distributional variations in marine crenarchaeotal membrane lipids: a new tool for reconstructing ancient sea water temperatures? Earth Planet. Sci. Lett. 204, 265–274.

Schouten, S., Hopmans, E.C., Sinninghe Damsté, J.S., 2004. The effect of maturity and depositional redox conditions on archaeal tetraether lipid palaeothermometry. Org. Geochem. 35, 567–571.

Schouten, S., Huguet, C., Hopmans, E.C., Sinninghe Damsté, J.S., 2007. Improved analytical methodology of the TEX_{86} paleothermometry by high performance liquid chromatography/atmospheric pressure chemical ionization–mass spectrometry. Anal. Chem. 79, 2940–2944.

Schouten, S., Pitcher, A., Hopmans, E.C., Villanueva, L., van Bleijswijk, J., Sinninghe Damsté, J.S., 2012. Distribution of core and intact polar glycerol dibiphytanyl glycerol tetraether lipids in the Arabian Sea Oxygen Minimum Zone: I: Selective preservation and degradation in the water column and consequences for the TEX_{86}. Geochim. Cosmochim. Acta 98, 228–243.

Schouten, S., Hopmans, E.C., Sinninghe Damsté, J.S., 2013. The organic geochemistry of glycerol dialkyl glycerol tetraether lipids: a review. Org. Geochem. 54, 19–61.
Sinninghe Damsté, J.S., Hopmans, E.C., Schouten, S., van Duin, A.C.T., Geenevasen, J.A.J., 2002. Crenarchaeol: the characteristic core glycerol dibiphytanyl glycerol tetraether membrane lipid of cosmopolitan pelagic crenarchaeota. J. Lipid Res. 43, 1641–1651.
Sinninghe Damsté, J.S., Rijpstra, W.I.C., Hopmans, E.C., Jung, M.Y., Kim, J.G., Rhee, S.K., Stieglmeier, M., Schleper, C., 2012. Intact polar and core glycerol dibiphytanyl glycerol tetraether lipids of Group I.1a and I.1b Thaumarchaeota in soil. Appl. Environ. Microbiol. 78, 6866–6874.
Strong, D.J., Flecker, R., Valdes, P.J., Wilkinson, I.P., Rees, J.G., Zong, Y.Q., Lloyd, J.M., Garrett, E., Pancost, R.D., 2012. Organic matter distribution in the modern sediments of the Pearl River Estuary. Org. Geochem. 49, 68–82.
Taylor, K.W.R., Huber, M., Hollis, C.J., Hernandez-Sanchez, M.T., Pancost, R.D., 2013. Re-evaluating modern and palaeogene GDGT distributions: implications for SST reconstructions. Global Planet. Chang. 108, 158–174.
Thompson, J.D., Gibson, T.J., Plewniak, F., Jeanmougin, F., Higgins, D.G., 1997. The CLUSTAL_X windows interface: flexible strategies for multiple sequence alignment aided by quality analysis tools. Nucleic Acids Res. 25, 4876–4882.
Turich, C., Freeman, K.H., Bruns, M.A., Conte, M., Jones, A.D., Wakeham, S.G., 2007. Lipids of marine Archaea: patterns and provenance in the water-column and sediments. Geochim. Cosmochim. Acta 71, 3272–3291.
Turich, C., Schouten, S., Thunell, R.C., Varela, R., Astor, Y., Wakeham, S.G., 2013. Comparison of TEX_{86} and U^{K}_{37} temperature proxies in sinking particles in the Cariaco Basin. Deep-Sea Res. I 78, 115–133.
Wang, P., Wei, Y., Li, T., Li, F., Meng, J., Zhang, C.L., 2014. Archaeal diversity and spatial distribution in the surface sediment of the South China Sea. Geomicrobiol J. 31 (1), 1–11.
Wei, Y., Wang, J., Liu, J., Dong, L., Li, L., Wang, H., Wang, P., Zhao, M., Zhang, C.L., 2011. Spatial variations in Archaeal lipids of surface water and core-top sediments in the South China Sea: implications for paleoclimate studies. Appl. Environ. Microbiol. 77, 7479–7489.
Weijers, J.W.H., Schouten, S., Spaargaren, O.C., Sinninghe Damsté, J.S., 2006. Occurrence and distribution of tetraether membrane in soils: implications for the use of the BIT index and the TEX_{86} SST proxy. Org. Geochem. 37, 1680–1693.
Weijers, J.W.H., Bernhardt, B., Peterse, F., Werne, J.P., Dungait, J.A.J., Schouten, S., Sinninghe Damsté, J.S., 2011a. Absence of seasonal patterns in MBT–CBT indices in mid-latitude soils. Geochim. Cosmochim. Acta 75, 3179–3190.
Weijers, J.W.H., Lima, K.H.L., Aquilina, A., Sinninghe Damsté, J.S., Pancost, R.D., 2011b. Biogeochemical controls on glycerol dialkyl glycerol tetraether lipid distributions in sediments characterized by diffusive methane flux. Geochem. Geophys. Geosyst. 12, Q10010. http://dx.doi.org/10.1029/2011GC003724.
Wuchter, C., Schouten, S., Wakeham, S.G., Sinninghe Damsté, J.S., 2006. Archaeal tetraether membrane lipid fluxes in the northeastern Pacific and the Arabian Sea: implications for TEX_{86} paleothermometry. Paleoceanography 21, PA4208. http://dx.doi.org/10.1029/2006PA001279.
Xie, W., Zhang, C.L., Zhou, X., Wang, P., 2014. Salinity-dominated change in community structure and ecological function of Archaea from the lower Pearl River to coastal South China Sea. Environ. Appl. Microbiol. Biotechnol. http://dx.doi.org/10.1007/s00253-014-5838-9.
Yang, G., Zhang, C.L., Xie, S., Chen, Z., Gao, M., Ge, Z., Yang, Z., 2013. Microbial glycerol dialkyl glycerol tetraethers from river water and soil near the Three Gorges Dam on the Yangtze River. Org. Geochem. 56, 40–50.
Zell, C., Kim, J.-H., Moreira-Turcq, P., Abril, G., Hopmans, E.C., Bonnet, M.P., Sobrinho, R.L., Sinninghe Damsté, J.S., 2013a. Disentangling the origins of branched tetraether lipids and crenarchaeol in the lower Amazon River: implications for GDGT-based proxies. Limnol. Oceanogr. 58, 343–353.
Zell, C., Kim, J.-H., Abril, G., Sobrinho, R.L., Dorhout, D., Moreira-Turcq, P., Sinninghe Damsté, J.S., 2013b. Impact of seasonal hydrological variation on the distributions of tetraether lipids along the Amazon River in the central Amazon basin: implications for the MBT/CBT paleothermometer and the BIT index. Front. Terr. Microbiol. 4. http://dx.doi.org/10.3389/fmicb.2013.00228.
Zell, C., Kim, J.-H., Hollander, D., Lorenzoni, L., Baker, P., Silva, C.G., Nittrouer, C., Sinninghe Damsté, J.S., 2014. Sources and distributions of branched and isoprenoid tetraether lipids on the Amazon shelf and fan: implications for the use of GDGT-based proxies in marine sediments. Geochim. Cosmochim. Acta 139, 293–312.
Zhang, Y.G., Zhang, C.L., Liu, X.L., Li, L., Hinrichs, K.U., Noakes, J.E., 2011. Methane Index: a tetraether archaeal lipid biomarker indicator for detecting the instability of marine gas hydrates. Earth Planet. Sci. Lett. 307, 525–534.
Zhang, C.L., Wang, J., Wei, Y., Zhu, C., Huang, L., Dong, H., 2012. Production of branched tetraether lipids in the lower Pearl River and estuary: effects of extraction methods and impact on bGDGT proxies. Front. Terr. Microbiol. 2. http://dx.doi.org/10.3389/fmicb.2011.00274.
Zhang, J., Bai, Y., Xu, S., Lei, F., Jia, G., 2013. Alkenone and tetraether lipids reflect different seasonal seawater temperatures in the coastal northern South China Sea. Org. Geochem. 58, 115–120.
Zhang, Y.G., Pagani, M., Liu, Z., 2014. A 12-million-year temperature history of the tropical Pacific Ocean. Science 344, 84–87.
Zhou, H., Hu, J., Spiro, B., Peng, P., Tang, J., 2014. Glycerol dialkyl glycerol tetraethers in surficial coastal and open marine sediments around China: indicators of sea SURFACE temperature and effects of their sources. Palaeogeogr. Palaeoclimatol. Palaeoecol. 395, 114–121.
Zhu, C., Weijers, J.W.H., Wagner, T., Pan, J.M., Chen, J.F., Pancost, R.D., 2011. Sources and distributions of tetraether lipids in surface sediments across a large riverdominated continental margin. Org. Geochem. 42, 376–386.